

# 8–13 $\mu\text{m}$ spectroscopy of NGC 253: a spatially resolved starburst

C. C. Dudley & C. G. Wynn-Williams

*Institute for Astronomy, University of Hawaii, 2680 Woodlawn Dr., Honolulu, Hawaii 96822, USA*

## ABSTRACT

NGC 253 is a nearby spiral galaxy that is currently undergoing a nuclear burst of star formation in a 100 pc diameter region. We present spatially resolved 8–13  $\mu\text{m}$  low-resolution spectra at four positions along the ridge of 8–13  $\mu\text{m}$  emission. We find that the relative strengths of the ionic, dust emission features, and dust continuum emission vary with position in the galaxy but can be accounted for everywhere without recourse to extinction by silicates. The brightest mid-infrared peak (which is displaced from the nucleus) has elevated levels of both continuum and 11.1–12.9  $\mu\text{m}$  “plateau” emission, indicative of dust heated within a photo-dissociation region. Spectra obtained over the course of 3 yr at the position of the brightest mid-infrared peak show no significant time variation.

**Key words:** dust – infrared: galaxies – galaxies: individual: NGC 253

## 1 INTRODUCTION

NGC 253 is a nearby ( $D \sim 3$  Mpc; Tully 1988) S(B)bc infrared bright galaxy whose infrared luminosity ( $\sim 2 \times 10^{10} L_{\odot}$ ; Tesesco & Harper 1980) is powered by a  $\sim 100$  pc diameter burst of star formation in the circumnuclear region. The infrared luminosity of NGC 253 exceeds that of the Milky Way by a factor of 2 with a larger relative fraction arising from the nuclear region. It thus provides an important proving ground to test our understanding of luminous infrared galaxies that are powered by compact starbursts. In these sources the higher luminosity per unit volume and the higher average density in the ISM may produce effects that are infrequently observed in star-forming regions in the Milky Way.

The central regions of NGC 253 are strongly affected by dust extinction at visual wavelengths. It is now generally agreed that the nucleus of the galaxy lies near to the point marked TH2 (Turner & Ho 1985) in Fig. 1, some  $3''$  (45 pc) away from the brightest infrared peak P1 (Sams et al. 1994; Kalas & Wynn-Williams 1994; Piña et al. 1992; Keto et al. 1993). The nature of P1 is unclear. Based on its mid-infrared properties, Kalas & Wynn-Williams (1994) suggested that it is a very young supernova remnant embedded in dust, while Watson et al. (1996), who observed it with the *Hubble Space Telescope*, suggested that it contains a young star cluster.

The 8–13  $\mu\text{m}$  spectral region provides useful information on the conditions in starbursts through thermal dust continuum emission, dust emission features, and ionic emission lines. The five strongest of the dust emission features occur at 3.3, 6.2, 7.7, 8.6, and 11.3  $\mu\text{m}$ . The features are

frequently attributed to polycyclic aromatic hydrocarbons (PAHs) (Puget & Léger 1989), but other laboratory analogues have also been proposed (e.g., Duley 1989; Sakata & Wada 1989; Ellis et al. 1994). PAH emission is widespread in the Galaxy. The features are observed in photo-dissociation regions (PDRs), reflection nebulae, and infrared cirrus, as well as in planetary nebulae. The ionic emission lines [Ar III], [S IV], and [Ne II], on the other hand, all arise in H II regions and can be used as indicators of both the hardness and strength of the ionizing continuum radiation in obscured regions.

Roche & Aitken (1985) used a  $7''6$  aperture to obtain 8–13  $\mu\text{m}$  spectra at two positions in the starburst in the nucleus of NGC 253. They found spectra that are broadly similar to those of many other star-forming galaxies, with contributions from dust continuum, PAH emission, and [Ne II]. They discuss evidence for silicate absorption in their spectra, a topic that we re-examine in this paper.

In this paper we present new 8–13  $\mu\text{m}$  spectra at four positions in the starburst nucleus along the mid-IR ridge of emission with particular emphasis on the peak P1, for which we have obtained observations over a 3-years baseline.

## 2 OBSERVATIONS AND DATA REDUCTION

### 2.1 Observations

The data were obtained using the cooled grating 10 and 20  $\mu\text{m}$  spectrometer CGS3 (Cohen & Davies 1995) at the United Kingdom Infrared Telescope (UKIRT) on Mauna

Kea. We used low-resolution mode ( $\frac{\lambda}{\Delta\lambda} \sim 60$ ) so that the entire 8–13  $\mu\text{m}$  atmospheric window was observed. Two separate interleaved grating positions are required to fully sample a spectrum with the 32-element linear detector array. Observations were performed by chopping with a 15'' throw in the northwest-southeast direction at a frequency of 5 Hz for 10 s, followed by a beam switch of equal duration. No more than 10 such cycles were performed before observing at the second grating position.

## 2.2 Pointing and astrometry

Fig. 1 shows the positions of our spectroscopic observations labeled as P0, P1, P2a, and P2b. These observations were obtained on three nights, one each in 1992, 1993, and 1994. Table 1 is a log of the observations giving the date, aperture size in arcseconds for full width at 10 per cent power, per-detector element on-source integration times in seconds, and for P0, P2a, and P2b the relative offset from the P1 observation in arcseconds. In Fig. 1, only the 2''.4 aperture is shown for P1. The central position of the CGS3 aperture with respect to the optical guide camera was established by using an automatic peak up routine on bright stars. In 1992, 1993, and 1994 the stars were HR 188, HR 8892, and HR 268, respectively, which are all within  $10^\circ$  of NGC 253. The telescope coordinate system was established by observing 2 to 3 Carlsburg Meridian Circle stars near the galaxy. In 1992, and 1994, we then slewed to P1, while in 1993, we peaked up manually on the P1 using the integrated flux between 8 and 13  $\mu\text{m}$ . We estimate that the 1992 and 1994 slew positions are accurate to 1''.5, while the offsets from the position of P1 are accurate to 0''.5.

The publication of the *Hipparcos* catalog has allowed a more precise determination of the position of the star used as an astrometric reference by Kalas & Wynn-Williams (1994). In Table 2 we give the proper-motion-corrected position for SAO 166579 based on the *Hipparcos* catalog. The position has not been corrected for parallax, which is the main source of the quoted error. The conversion to the FK4 system was performed using the routine BPRECESS provided with IDL version 5 using the epoch keyword. The position is consistent with the proper motion corrected position derived from the FK4 format PPM catalog (available from the NASA Astrophysics Data System), which is  $0^\circ.02$  east and  $1''.34$  south of the SAO position used by Kalas & Wynn-Williams (1994). Table 2 also gives the revised positions for Kalas & Wynn-Williams's Peaks 1–3, the radio positions of TH2 and TH7 (Turner & Ho 1985), and the positions of two red objects observed by Watson et al. (1996). In Table 2 we see that the revised position for Kalas & Wynn-Williams's Peak 1 is now consistent with TH7 and that their Peak 2 is now about  $1\sigma$  distant from TH2. The positions of Kalas & Wynn-Williams' Peaks 1 and 3 are consistent with Watson et al.'s Bright blob and Spot *a*, respectively; if Peak 1 and their Bright blob are brought into coincidence, then the positions of Peak 3 and Spot *a* agree within  $0^\circ.01$  in  $\alpha$  and  $0''.02$  in  $\delta$ , within the estimated internal accuracy of the two observations.

## 2.3 Data Reduction

Our spectra have been flux calibrated against bright stars. In 1992, 1993, and 1994, we used HR 1457 ( $N=-3.03$ ; Tokunaga 1984), HR 7001 ( $N=0.00$ ), and HR 7949 ( $N=0.0$ ; assumed), respectively. Wavelength-dependent variations in instrumental response and atmospheric transmission were removed by dividing the object spectra by stellar spectra and multiplying by a model Planck function. In 1992 and 1993, all spectra were first corrected to 1 airmass using atmospheric transmission curves based on data collected during each observing run. In 1994, the same star was used as a spectral and flux calibrator and was observed within 0.1 airmass of the source. In 1992, HR 0617 was used for spectroscopic calibration with an assumed temperature of 4780 K; in 1993, HR 0188 was used with an assumed temperature of 4690 K; and for the 1994 observations, the assumed temperature for HR 7949 was 4690 K. All the spectral standards are spectral type K0 or earlier so that they should not be strongly affected by SiO absorption (Cohen et al. 1992a). Deviation from our model Planck function due to wavelength-dependent  $\text{H}^-$  opacity is also likely to be small (Cohen et al. 1992b). We estimate our absolute photometric accuracy to be better than 10 per cent.

Wavelength calibration was based upon observations of a Kr lamp as described by Hanner, Brooke & Tokunaga (1995). Due to year-to-year variations in instrumental setup, which resulted in slightly different wavelength scales for our spectra, we have resampled all our spectra to a common wavelength scale using Gaussian weighting with  $\sigma = 0.06\ \mu\text{m}$ . Thus, the individual data presented below are nearly but not entirely independent of their spectral neighbors. We found no significant difference between the spectra obtained at P1 over the 3 yr, so we have combined them to enhance the signal-to-noise ratio. Given the compact size  $\leq 1''.2$  (Keto et al. 1993) of P1 between 8 and 13  $\mu\text{m}$ , it is not surprising that spectra obtained with our two aperture sizes should agree, and this agreement can be taken as evidence that P1 was reasonably well centered all 3 yr.

Due to year-to-year variations in instrumental setup, which resulted in slightly different wavelength scales for our spectra, we have resampled all our spectra to a common wavelength scale using Gaussian weighting with  $\sigma = 0.06\ \mu\text{m}$ . Thus, the individual data presented below are nearly but not entirely independent of their spectral neighbors. We found no significant difference between the spectra obtained at P1 over the 3 yr, so we have combined them to enhance the signal-to-noise ratio. Given the compact size  $\leq 1''.2$  (Keto et al. 1993) of P1 between 8 and 13  $\mu\text{m}$ , it is not surprising that spectra obtained with our two aperture sizes should agree, and this agreement can be taken as evidence that P1 was reasonably well centered all 3 yr.

Wavelength calibration was based upon observations of a Kr lamp as described by Hanner, Brooke & Tokunaga (1995). Due to year-to-year variations in instrumental setup, which resulted in slightly different wavelength scales for our spectra, we have resampled all our spectra to a common wavelength scale using Gaussian weighting with  $\sigma = 0.06\ \mu\text{m}$ . Thus, the individual data presented below are nearly but not entirely independent of their spectral neighbors. We found no significant difference between the spectra obtained at P1 over the 3 yr, so we have combined them to enhance the signal-to-noise ratio. Given the compact size  $\leq 1''.2$  (Keto et al. 1993) of P1 between 8 and 13  $\mu\text{m}$ , it is not surprising that spectra obtained with our two aperture sizes should agree, and this agreement can be taken as evidence that P1 was reasonably well centered all 3 yr.

## 3 RESULTS

In Fig. 2 we present our spectra of the starburst region of NGC 253. The panels are labeled in accordance with Fig. 1 and Table 1. We note that certain features are apparent in all the spectra. The brightest emission features are the [Ne II] forbidden line at 12.8  $\mu\text{m}$  and the PAH emission feature at 11.3  $\mu\text{m}$ . The 8.6- $\mu\text{m}$  PAH feature is also present in each spectrum. The continuum emission has a broad minimum near 10  $\mu\text{m}$ ; we shall argue in Section 4.1 that this 'continuum' is actually a combination of a true thermal continuum between 10 and 13  $\mu\text{m}$  and the long wavelength shoulder of the 7.7- $\mu\text{m}$  PAH emission feature. Each spectrum also shows signs of an elevated level of emission between 11.1 and 12.9  $\mu\text{m}$ . This so-called "plateau" emission has been previously observed in the Orion Bar photo-dissociation region (PDR) by Roche, Aitken & Smith (1989). There are no signs of the 10.5- $\mu\text{m}$  [S IV] or 9.0- $\mu\text{m}$  [Ar III] forbidden emission lines in any spectrum.

As a check on our calibration, we have computed the average flux density between 11.15 and 12.25  $\mu\text{m}$  of the bright source P1. Our value of  $4.7 \pm 0.1\ \text{Jy}$  is in good agreement with the estimate of Piña et al. (1992) of 4.8 Jy.

## 4 DISCUSSION

Our discussion will first concentrate on two progressively more detailed fits to our spectra culminating with a table of measurements of spectral feature properties. We will then discuss the question of silicate absorption in NGC 253, followed by an analysis of the strengths of the ionic emission lines. Finally we discuss the possible origins of the continuum emission and the spatial variations seen in our spectra.

We fit the features in our spectra in two stages. First we apply a two-component model to the whole of each spectrum consisting of a thermal continuum underlying PAH emission. This procedure allows us to test whether or not silicate absorption is present in these spectra by examining the agreement of the observations with what the fits predict near  $8\ \mu\text{m}$ . Second, we decompose the emission above the thermal continuum longward of  $11\ \mu\text{m}$  into three components: PAH feature emission, [Ne II] emission, and plateau emission.

### 4.1 Initial fitting: Continuum and $11.3\ \mu\text{m}$ feature

Our initial procedure is to fit the  $10\text{--}13\ \mu\text{m}$  spectrum of each region to a combination of thermal blackbody and  $11.3\text{-}\mu\text{m}$  PAH emission feature, and then compare this model's predicted  $8\text{--}10\ \mu\text{m}$  emission with the observations. The procedure is similar to that employed for Arp 299C in our earlier paper (Dudley & Wynn-Williams 1993) except that the continuum is now estimated solely from the spectra themselves rather than in conjunction with longer wavelength photometric data. For a PAH template we use the Orion Bar data of Roche et al. (1989) degraded in spectral resolution to match the present data. The particular spectrum we use is that taken at Beckin et al.'s (1976) position 4, following Roche (1989) so that a prediction can be made of the strength of  $8\text{--}10\ \mu\text{m}$  emission.

In Fig. 2, the solid lines are Planck function fits to the continuum between  $10$  and  $11\ \mu\text{m}$  and at  $13.2\ \mu\text{m}$  and the dotted line shows the Orion Bar spectrum scaled so that the intensity of Orion Bar emission around the  $11.3\text{-}\mu\text{m}$  PAH feature between  $10.9$  and  $11.7\ \mu\text{m}$  matches that found above the continuum fits in our spectra. The shaded regions in Fig. 2 represent the reasonable range in the predicted  $8\text{--}10\ \mu\text{m}$  emission based on the  $10\text{--}13\ \mu\text{m}$  fits. They are bounded on the bottom by the Orion Bar spectrum of Bregman et al. (1989) with the same scaling relative to the Roche et al. (1989) spectrum as that adopted by Roche (1989), and on the top by the same multiplied by a factor of 2. The shaded region reflects the observation that there is a factor of 2 scatter in the ratio of the intensities of the  $11.3$  to  $7.7+8.6\ \mu\text{m}$  features reported by Zavagno, Cox, & Baluteau (1992) in observations of galactic H II regions. Of the sources they analyze, the Orion Bar is among those with the strongest  $11.3\text{-}\mu\text{m}$  features relative to the  $7.7+8.6\text{-}\mu\text{m}$  features. As seen in Fig. 2, the simple model described in the last paragraph provides an acceptable description of the gross features of all the spectra of NGC 253 we obtained. We therefore conclude, leaving aside the ionic [Ne II] emission line, that the  $8\text{--}13\ \mu\text{m}$  spectrum NGC 253 can be explained by a thermal continuum rising towards longer wavelengths, plus a PAH spectrum scaled to the intensity of the  $11.3\text{-}\mu\text{m}$  feature. Thus the minimum near  $9.7\ \mu\text{m}$  need not be produced by silicate

absorption; we discuss the limits on silicate absorption in Section 4.3.

The color temperatures and  $13.2\text{-}\mu\text{m}$  continuum flux densities of the four measured regions are given in rows 1–2 of Table 3. As a check on the appropriateness of modeling the continuum in this manner, we extrapolate the results of the fits to  $19.5\ \mu\text{m}$  and compare the extrapolations with the data given by Piña et al. (1992). For IRS 1, they report a  $19.5\ \mu\text{m}$  flux density of  $24.8\ \text{Jy}$ , which is within 6% of our extrapolation at P1 of Fig. 1. For all the other positions in Fig. 1, our extrapolations over predict the contours of their  $19.5\ \mu\text{m}$  deconvolved map. The largest over predictions (a factor of 2) occur at P0 and P2b where we measure the lowest values of the color temperature. There are several possible explanations for this. First, notwithstanding Piña et al.'s efforts to deconvolve their map, there may remain important differences between their beam size and ours. Second, a blackbody may not be the best representation for the continuum; a  $\lambda^{-1}$  or  $\lambda^{-1.5}$  emissivity law gives a much better fit to their map. Third, some silicate absorption may have led to an underestimate of the continuum temperature at these positions. The silicate optical depth required ( $\tau_{\text{sil}}(9.7) \sim 0.7$ , with  $T_{\text{cont}} = 150\ \text{K}$ ) does not exceed the limits we set on the silicate optical depth in section 4.2.

### 4.2 Detailed fitting: The plateau emission

In the Orion Bar, the [Ne II] emission,  $11.3\text{-}\mu\text{m}$  PAH feature, and plateau all have different spatial distributions (Roche et al. 1989); we have chosen to fit these three components separately after first subtracting the thermal continuum.

Our fitting method is quite similar to that employed by Roche et al. (1989) to analyse the Orion Bar. There are two main differences: (1) In the Orion Bar, a feature at  $12.7\ \mu\text{m}$  shows the same spatial variation as the  $11.3\text{-}\mu\text{m}$  feature (Roche et al. 1989), but due to our lower spectral resolution, the  $12.7\text{-}\mu\text{m}$  feature cannot be independently measured here. We have therefore assumed a fixed ratio between the intensities of the  $11.3\text{-}$  and  $12.7\text{-}\mu\text{m}$  features of 2.4 based on the Orion Bar results. (2) We have chosen a plateau spectral profile that is stronger at longer wavelengths in  $F_{\lambda}$  rather than the flatter profile employed by Roche et al. (1989). While our profile has the same spectral width as theirs, it rises linearly in wavelength and is twice as strong at  $12.5\ \mu\text{m}$  than at  $11.5\ \mu\text{m}$ . This shape was chosen to match the shape of the plateau emission in the P1 spectrum, which has the highest signal-to-noise ratio.

We first fitted and subtracted the plateau by matching intensity between  $11.6$  and  $12.2\ \mu\text{m}$  for the data and the profile. We then matched intensities and subtracted an assumed Gaussian profile centered at  $11.3\ \mu\text{m}$  and with  $\sigma = 0.13\ \mu\text{m}$ , where the matching occurred between  $11.0$  and  $11.4\ \mu\text{m}$ ; a Gaussian centered on  $12.7\ \mu\text{m}$  with width  $\sigma = 0.26\ \mu\text{m}$  was also subtracted as described previously. Finally the intensity of the [Ne II] feature was measured between  $12.6$  and  $13.0\ \mu\text{m}$ . These procedures left residuals that were not significantly different from zero except in the P1 and the P2a spectra, where an apparent feature at  $11.5\ \mu\text{m}$  of intensities  $1.3 \pm 0.4$  and  $1.4 \pm 0.4 \times 10^{-15}\ \text{W m}^{-2}$ , respectively, measured between  $11.3$  and  $11.7\ \mu\text{m}$  remained. Since such a feature has been observed in some Galactic sources exhibiting PAH emission (Roche, Aitken & Smith 1991a),

these features could be real, but since we have modified the shape of our plateau model from that employed by Roche et al. (1989), we do not make any strong claim for this. This fitting procedure also produced a lower estimate of the 11.3- $\mu\text{m}$  intensity than the model used to produce Fig. 2. The largest reduction occurred for P1, where the new 11.3- $\mu\text{m}$  intensity is about 80 per cent of that used in Fig. 2. About half of this reduction is due to plateau subtraction, and half is due to our effort to exclude flux from the apparent feature at 11.5  $\mu\text{m}$ .

We summarize the results of the fits shown in Fig. 3 in rows 3–5 of Table 3. Rows 6 and 7 are limits on the intensities of two additional ionic emission lines: 8.99- $\mu\text{m}$  [Ar III], and 10.5- $\mu\text{m}$  [S IV]. The equivalent widths of the 11.3- $\mu\text{m}$  PAH feature and the 12.8- $\mu\text{m}$  [Ne II] line in rows 8 and 9 are based on the intensities in rows 3 and 5 and a model continuum that includes contributions from both the thermal continuum given in rows 1 and 2 and a plateau contribution, and in the case of [Ne II], an assumed 12.7- $\mu\text{m}$  feature contribution. Row 10 gives the intensity ratios between the plateau and 11.3- $\mu\text{m}$  PAH features. The errors given in Table 3 are 1  $\sigma$  while upper limits are 3  $\sigma$ .

There are few spectra of galaxies available with sufficient signal-to-noise ratios to detect the 11.1–12.9  $\mu\text{m}$  plateau feature, so it is difficult to make comparisons with other galaxies, although plateau emission is clearly present in the two *Infrared Space Observatory* spectra of the antennae galaxy system presented by Vigroux et al. (1996).

Most of what is known about the plateau emission is based on observations of the Orion Bar region. Roche et al. (1989) have made spatially resolved observations of the Orion Bar. Their observations of the ratio of the intensities of the plateau emission to 11.3- $\mu\text{m}$  feature varies between 1.5 and 6.7. The lowest value is found on the visible Bar itself (Becklin et al.’s (1976) position 4), which also behaves to some degree as a reflection nebula, and the highest value is found at a position 20'' south, well within the dense part of the molecular cloud. At the position where the plateau emission is the strongest (5'' south of position 4), the ratio has a value of 2.7. The range of values for this ratio listed in Table 3 for NGC 253 falls within the range of values we have just calculated. Of particular interest are the high values of the ratio seen at P1 and P2a that can only be approximated by the southern most values in the Orion Bar. These values may show that conditions similar to those occurring in the deep layer of the Orion Bar PDR are more prevalent than those occurring adjacent to the ionization front.

### 4.3 Limits on Silicate Absorption

Aitken & Roche (1984) have proposed a method of determining the amount of silicate absorption required for spectra that include PAH emission based on observations of galactic planetary nebulae and employing the equivalent width of either the 11.3- or 8.6- $\mu\text{m}$  features. Given the factor of 2 dispersion in the observed 11.3- to 7.7+8.6- $\mu\text{m}$  features intensity ratio in galactic H II regions, we prefer to set an upper limit on the amount of true thermal continuum that might be present at 8  $\mu\text{m}$  and thus an upper limit on  $\tau_{\text{Sil}}(9.7)$

where

$$\tau_{\text{Sil}}(9.7) = \ln \left( \frac{F_{\lambda}(8) + F_{\lambda}(13)}{2 \times F_{\lambda}(9.7)} \right)$$

(Aitken & Jones 1973). We therefore take the difference between the lower boundary of the shaded region at 8  $\mu\text{m}$  (less our model continuum at 8  $\mu\text{m}$ ) and the spectra as a rough limit on the amount of continuum that can contribute to the flux at 8  $\mu\text{m}$ . This value, along with the model continuum flux at 9.7 and 13  $\mu\text{m}$ , combine to give an upper limit on  $\tau_{\text{Sil}}(9.7)$  in the equation of Aitken & Jones (1973). These limits are given in row 11 of Table 3.

We find that our upper limits on  $\tau_{\text{Sil}}(9.7)$  are in agreement with the  $\tau_{\text{Sil}}(9.7)$  reported by Roche & Aitken (1985) of  $1.4 \pm 0.3$  based on the method of Aitken & Roche (1984) for NGC 253, given the very different aperture sizes we have employed. We note that these limits on  $\tau_{\text{Sil}}(9.7)$  apply to silicate absorption by cold dust, but not to the optical depth in dust that is emitting between 8–13  $\mu\text{m}$ . The limit for P1 is consistent with the amount of extinction estimated by Watson et al. (1996) based on  $V - I$  colors under the assumption that  $A_V = 15 \times \tau_{\text{Sil}}(9.7)$  (Aitken 1981).

### 4.4 Ionic Lines

The presence and absence of ionic lines in our spectra allow us to derive properties of the ionized gas within NGC 253.

In all four of the spectra shown in Fig. 2, the [Ne II] emission line is clearly detected, but the [Ar III] and [S IV] lines are not. Of these two lines the limits on I([S IV]) in Table 3 are probably more reliable given the systematic errors introduced by both the presence of the shoulder of the 7.7+8.6- $\mu\text{m}$  features and the adjacent telluric O<sub>3</sub> absorption that could affect the continuum estimate for the 8.99- $\mu\text{m}$  [Ar III]. We therefore concentrate on what can be learned from the limits on I([S IV]) emission. The ratio of I([S IV]) to I([Ne II]) is sensitive to the hardness of the  $L_{\text{Ycont}}$  radiation field ionizing the H II regions producing the emission and thus to the presence of very hot stars. Assuming a number abundance ratio of S to Ne of 0.27,  $n_e \sim 10^3 - 10^4 \text{ cm}^{-3}$ , and  $L_{\text{Ycont}}$  fluxes following the models of Kurucz (1979), Rubin (1985) gives ratios of I([S IV])/I([Ne II]) of 0.02 and 1 for exciting stars of  $T_{\text{eff}} = 33,000$  and 36,000 K, respectively. Our upper limits on I([S IV]) imply that I([S IV])/I([Ne II]) < 0.33, 0.09, 0.14, and 0.13 for each of the spectra P0, P1, P2a, and P2b, respectively. Thus the nondetection of the [S IV] line suggests that the bulk of the stars producing ionizing radiation have  $T_{\text{eff}} < 36,000$  K. The strongest limit is seen at P1, where a finer grid of models than those examined here would be useful. The limit on  $T_{\text{eff}}$  holds even if  $\tau_{\text{Sil}} \sim 1.2$ , which would increase our upper limits on I([S IV])/I([Ne II]) by a factor of 1.7 based on the Mathis (1990) extinction curve with  $R \sim 3$  supplemented by a  $\mu$  Cep silicate profile matching our spectral resolution (see Dudley & Wynn-Williams 1997 for details.)

The [Ne II] emission may be compared with observations at other wavelengths. Puxley & Brand (1995) measure a Br $\gamma$  flux of  $0.18 \times 10^{-15} \text{ W m}^{-2}$  at P1 using a 3'' slit oriented along the galaxy’s major axis. This gives I(Br $\gamma$ )/I([Ne II]) = 0.015 which is within 25 per cent of the prediction of Dudley & Wynn-Williams (1993) of 0.011 but is quite low compared to the models of Rubin (1985) in the range of  $T_{\text{eff}}$

suggested by the upper limit on  $I([\text{SIV}])$ , which predict a ratio of 0.048. Different assumptions about Ne abundance, Brackett to Balmer series intensity ratios, and the  $[\text{Ne II}]$  collision strength can account for about half of the discrepancy between the two predictions. On the other hand, applying the reddening deduced by Watson et al. (1996) towards P1 to the prediction of Rubin (1985) gives good agreement with the observed ratio. Applying the  $I([\text{Ne II}])$  to  $I(\text{Br}\gamma)$  conversion factor of Dudley & Wynn-Williams (1993) followed by a further conversion using the  $\text{Br}\gamma$  intensity to 6-cm free-free flux density ratio of  $8 \times 10^{11}$  Hz from Wynn-Williams (1982) to the observed  $[\text{Ne II}]$  intensity predicts a 6-cm flux density of 17 mJy, which is not too different from the observed value of about 10 mJy for TH 7 (Ulvestad & Antonucci 1997). The 6 to 2 cm spectral index of this source is  $\alpha = -0.24$  ( $S_\nu \propto \nu^\alpha$ ), intermediate between optically thin free-free and synchrotron indices, suggesting that both processes contribute to the radio emission.

For P2a, at the nucleus of the galaxy, the predicted  $\text{Br}\gamma$  flux based on the  $[\text{Ne II}]$  flux (Dudley & Wynn-Williams 1993) is  $0.10 \times 10^{-15}$  W m<sup>-2</sup>, which is a factor of 2 lower than the  $0.24 \times 10^{-15}$  W m<sup>-2</sup> observed by Puxley & Brand (1995). This may indicate that there is an ionizing source associated with the nonthermal radio source (TH2) that produces  $\text{Br}\gamma$  emission that is not mirrored in the  $[\text{Ne II}]$  emission, possibly because the ionized gas density is too high ( $n_e > 10^5$  cm<sup>-3</sup>) to produce as much  $[\text{Ne II}]$  emission. This speculation is not supported, however, when using the ratio of Rubin (1985) which overpredicts the observed  $\text{Br}\gamma$  flux by a factor of 2. As in the case of P1, this effect might also be accounted for by reddening. Both comparisons are beset by possible aperture differences, an unknown Ne abundance, and uncertainties in determining the  $[\text{Ne II}]$  intensity due to our subtraction of an assumed 12.7- $\mu\text{m}$  PAH feature so that only firm conclusion that can be drawn is that the  $\text{Br}\gamma$  and  $[\text{Ne II}]$  are in agreement within a factor of 4 under the assumption that they both arise from H II regions.

The 6-cm radio continuum in P2a is about 40 mJy (Ulvestad & Antonucci 1997), stronger than the free-free emission predicted from the intensities of either  $[\text{Ne II}]$  or  $\text{Br}\gamma$ , which amount to about 13 mJy. This is consistent with the statement of Turner & Ho (1985) that the 2-cm radio continuum emission from TH2 must be due to nonthermal emission since its brightness temperature of  $10^5$  K is too high to be due to free-free emission from H II regions. On the other hand, the amount of free-free emission that we would predict by substituting the  $[\text{Ne II}]$  to  $\text{Br}\gamma$  conversion factor given by Rubin (1985) but retaining the  $\text{Br}\gamma$  to 6-cm flux density factor adopted from Wynn-Williams (1982) gives good agreement with the observed 6-cm emission.

#### 4.5 Continuum emission

In standard Case B recombination theory, radio free-free emission, Brackett series recombination line emission, and  $[\text{Ne II}]$  emission all trace the number of ionizing photons with little sensitivity to electron temperature and density for the values typical of H II regions. Thus,  $[\text{Ne II}]$  emission may be used to predict the amount of grain emission due to trapped Ly $\alpha$  heating in H II regions while avoiding the possible problems of extinction at short wavelengths and non-thermal emission at radio wavelengths. Taking the  $\text{Br}\gamma$ -to-

$[\text{Ne II}]$  intensity ratio predicted by Dudley & Wynn-Williams (1993) and a  $\text{Br}\gamma$  intensity to 6-cm free-free flux density ratio from Wynn-Williams (1982), we predict a free-free flux density at 6 cm of between 5 and 17 mJy for the four spectra. Using the continuum temperatures given in Table 3, we may then use formula A4 of Genzel et al. (1982) to predict the expected flux density at 13.2  $\mu\text{m}$  due to trapped Ly $\alpha$  heating of dust and compare these predictions with the observed values given in Table 3. We find that the observed continuum exceeds these predictions by large factors of 30–50. We therefore conclude that Ly $\alpha$  heating fails to account for the 10–13  $\mu\text{m}$  continuum in any of our spectra.

#### 4.6 Spatial Variations

Before discussing the possible reasons for spatial variations among our spectra of NGC 253 we need to review the status of the compact source P1.

In this paper we have already shown that the 8–13  $\mu\text{m}$  spectrum of P1 is consistent with a combination of thermal dust emission and Orion Bar-like emission along with  $[\text{Ne II}]$  emission similar to that seen in starburst galaxies (see Fig. 2). Further, we observed no time variation in the 8–13  $\mu\text{m}$  spectrum over the 3 yr that we observed it. In view of the absence of time variations, and of Watson et al.’s (1996) *HST* detection of a star cluster spatially coincident with P1, the suggestion of Kalas & Wynn-Williams (1994) that P1 is a dust-embedded recent supernove is probably incorrect.

Our spectrum of P1 can provide a new estimate of the 1–1000  $\mu\text{m}$  luminosity of the source based on the color temperature and flux of the continuum. A 145-K blackbody with a 13.2- $\mu\text{m}$  flux density of 6.7 Jy at a distance of 3 Mpc has a luminosity of  $1.6 \times 10^9 L_\odot$ . We recall the agreement noted in section 4.1 between this extrapolation and the 19.5  $\mu\text{m}$  data of Piña et al. (1992). This luminosity estimate for P1 is in good agreement with the estimate of Watson et al. (1996) of  $1.8 \times 10^9 L_\odot$  which is based on their estimate of the fraction of the flux due to P1 in the 12.5- $\mu\text{m}$  map of Keto et al. (1993) applied to the  $L_{10-350\mu\text{m}}$  for the inner 30'' of NGC 253 given by Telesco & Harper (1980). However, our estimate of the flux due to P1 in the Keto et al. (1993) map is a factor of 2.3 larger than that of Watson et al. (1996), so the agreement is largely fortuitous. By either estimate, P1 provided  $\sim 8$  per cent of the infrared luminosity of the galaxy.

The 11.3- $\mu\text{m}$  feature is clearly present in all our spectra but shows a large variation in EW. This is consistent with the observations of the related 3.3- $\mu\text{m}$  feature reported by Kalas & Wynn-Williams (1994), where it was found to be relatively weak compared to the continuum at P1. The EW of the 11.3- $\mu\text{m}$  feature ranges over a factor of 4 and is anti-correlated with the continuum temperature, while the ratio of the intensities of  $[\text{Ne II}]$  to 11.3- $\mu\text{m}$  feature cover a factor of 2 and all fall within the range reported by Roche et al. (1991b) for 19 galaxies showing both features.

The young star cluster model for P1 leads, at least qualitatively, to a plausible explanation for the differences seen between the spectrum at P1 (and to some extent P2a) and elsewhere in the galaxy. Because the interstellar radiation field is presumably stronger within the compact P1 star cluster than the interstellar radiation field elsewhere, regular dust grains will be heated to higher temperatures as is

observed (Table 3). Since we have already shown that Ly $\alpha$  heating is insufficient to heat the dust, we need to invoke direct dust heating by starlight. The prominence of the plateau emission in the spectrum of P1 suggests that emission that arises in PDRs is particularly important in P1, so we suspect that the dust that gives rise to the continuum emission is likely to come mainly from the outer layers of molecular clouds exposed to the starlight. The relative importance of large-grain (equilibrium) heating and small-grain (transient) heating is difficult to establish solely with the new data presented here.

## 5 CONCLUSIONS

We have presented spatially resolved 8–13  $\mu\text{m}$  spectroscopy of the nuclear region of the starburst galaxy NGC 253. We find that high-mass star formation explains the observed spectra through a combination of PAH emission, [Ne II] emission, and thermal continuum with little need to invoke absorption by cold dust greater than  $A_V \sim 15$ .

Based on the revised astrometry of Kalas & Wynn-Williams (1994) we identify P1 with an optical red object observed by Watson et al. (1996) and with the 2-cm radio source TH7 observed by Turner & Ho (1995).

We report the measurement of a low-contrast but high-intensity plateau of PAH emission in the 11.1–12.9  $\mu\text{m}$  range, and identify it with emission observed in PDRs in the vicinity galactic H II regions.

We set a limit on the effective temperature of the integrated emission from stars sampled by our spectra to be less than 36,000 K based on the comparison of I([Ne II]) and upper limits on I([S IV]) under the assumption that the dust optical depth is not very large at 10.5  $\mu\text{m}$ .

We compare I([Ne II]) with I(Br $\gamma$ ) and radio continuum emission from P1, and find reasonable agreement with standard recombination theory, while for P2a the radio continuum emission is probably too strong to be due to H II regions.

We examine the relative intensities of 11.3- $\mu\text{m}$  PAH emission feature, plateau emission, and the [Ne II] emission line, and the continuum intensity and color temperature and find that while the [Ne II] and 11.3  $\mu\text{m}$  PAH emission are roughly proportional, as observed in other starburst galaxies, the 11.3  $\mu\text{m}$  PAH feature and plateau emission show a larger range of variation with respect to each other. We suggest that enhanced plateau emission is due to the predominance of conditions more similar to the depths of PDRs than regions adjacent to ionization fronts.

## ACKNOWLEDGMENTS

We would like to thank the UKIRT staff—Joel Aycock, Dolores Walther, and Thor Wold—for assistance at the telescope, and Tom Geballe, for helpful discussions. UKIRT is operated by the Joint Astronomy Centre on behalf of the U.K. Particle Physics and Astronomy Research Council. F. Crifo gave us very helpful advice concerning the comparative reliability of different astrometric catalogs. Many members of the Institute for Astronomy have benefited this work through discussion and sharing of work in progress. A few are Dave Sanders, Bob Joseph, Klaus Hodapp, Alan Tokunaga, Joe Hora, Tom Greene, Paul Kalas, and Jason Surace; we thank these and others. This work has been partially

supported by NSF grant ASTR-8919563, and NASA grant NAGW-3938. The NASA Extragalactic Database, (NED) has been a constant aid. It is run by the Jet Propulsion Laboratory, California Institute of Technology, under contract with the National Aeronautics and Space Administration. This work has also made use of NASA's Astrophysics Data System Abstract Service and Catalog database.

Table 1. Observing Log for NGC 253

Date (UT)	Aperture (")	Sources Observed	Time on Source (s)	Offset from P1
1992 Oct 15	3.26	P1	200	
		P2b	500	2''7E 2''0N
1993 Aug 31	2.40	P0	500	1''8W 2''0S
		P1	350	
		P2a	500	1''8E 2''0N
1994 Aug 28	3.26	P1	100	

Table 2. Positions of Bright Peaks in NGC 253

Publication	$\lambda$	Source Name	Position (1950)	
			$\alpha = 00^{\text{h}} 45^{\text{m}}$	$\delta = -25^{\circ} 33'$
Kalas & Wynn-Williams	4.8 $\mu\text{m}$	Peak 1	$05^{\text{s}}.632 \pm 0.037$	$41''.34 \pm 0.5$
Turner & Ho	2 cm	7	$05^{\text{s}}.626$	$41''.23$
Watson et al.	0.6 $\mu\text{m}$	Bright blob	$05^{\text{s}}.58 \pm 0.02$	$41''.08 \pm 0.3$
Kalas & Wynn-Williams	4.8 $\mu\text{m}$	Peak 2	$05^{\text{s}}.782 \pm 0.037$	$39''.50 \pm 0.5$
Turner & Ho	2 cm	2	$05^{\text{s}}.795$	$38''.95$
Kalas & Wynn-Williams	4.8 $\mu\text{m}$	Peak 3	$06^{\text{s}}.08 \pm 0.037$	$35''.89 \pm 0.5$
Watson et al.	0.6 $\mu\text{m}$	Spot <i>a</i>	$06^{\text{s}}.03 \pm 0.02$	$35''.61 \pm 0.3$
<i>Hipparcos</i>	...	SAO 166579	$\alpha = 00^{\text{h}} 45^{\text{m}}$ $7^{\text{s}}.4638 \pm 0.0004$	$\delta = -25^{\circ} 40'$ $3''.677 \pm 0.005$

Table 3. Spectral Measurements of NGC 253

Property	Position			
	P0	P1	P2a	P2b
$T_{\text{cont}}$ [K]	$119^{+9}_{-8}$	$145^{+2}_{-2}$	$136^{+4}_{-4}$	$119^{+5}_{-5}$
$F_{\nu}(13.2 \mu\text{m})$ [Jy]	$1.7 \pm 0.1$	$6.7 \pm 0.1$	$4.3 \pm 0.1$	$3.3 \pm 0.1$
$I_{11.3\mu\text{m}}$ [ $10^{-15} \text{ W m}^{-2}$ ]	$3.3 \pm 0.4$	$6.0 \pm 0.3$	$6.7 \pm 0.3$	$5.9 \pm 0.4$
$I_{[\text{NeII}]}$ [ $10^{-15} \text{ W m}^{-2}$ ]	$3.9 \pm 0.8$	$12.2 \pm 0.8$	$9.0 \pm 0.8$	$10.9 \pm 0.9$
$I_{11.1-12.9\mu\text{m}}$ [ $10^{-15} \text{ W m}^{-2}$ ]	$6 \pm 2$	$30 \pm 2$	$25 \pm 2$	$17 \pm 2$
$I_{[\text{ArIII}]}$ [ $10^{-15} \text{ W m}^{-2}$ ]	$<1.3$	$<1.1$	$<1.3$	$<1.3$
$I_{[\text{SiIV}]}$ [ $10^{-15} \text{ W m}^{-2}$ ]	$<1.3$	$<1.1$	$<1.3$	$<1.3$
EW 11.3 [ $\mu\text{m}$ ]	$0.22 \pm 0.02$	$0.075 \pm 0.004$	$0.14 \pm 0.01$	$0.19 \pm 0.01$
EW [Ne II] [ $\mu\text{m}$ ]	$0.13 \pm 0.03$	$0.09 \pm 0.01$	$0.11 \pm 0.01$	$0.17 \pm 0.01$
$\frac{I_{11.1-12.9\mu\text{m}}}{I_{11.3\mu\text{m}}}$	$2.0 \pm 0.6$	$5.0 \pm 0.5$	$3.8 \pm 0.3$	$2.9 \pm 0.3$
$\tau_{\text{SiI}}(9.7)$	$<1.3$	$<0.7$	$<0.8$	$<1.6$

## REFERENCES

- Aitken D. K., 1981, in Wynn-Williams C. G., Cruikshank D. P., eds, Proc. IAU Symp. 96, Infrared Astronomy, Reidel, Dordrecht, p. 207
- Aitken D. K., Jones B., 1973, ApJ, 184, 127
- Aitken D. K., Roche P. F., 1984, MNRAS, 208, 751
- Becklin E. E., Neugebauer G., Beckwith S., Gatley I., Matthews K., Sarazin C., Werner M. W., 1976, ApJ, 207, 770
- Bregman J. D., Allamandola L. J., Tielens A. G. G. M., Geballe T. R., Witteborn F. C., 1989, ApJ, 344, 791
- Cohen M., Davies J. K., 1995, MNRAS, 276, 715
- Cohen M., Walker R. G., Barlow M. J., Deacon J. R., 1992b, AJ, 104, 1650
- Cohen M., Witteborn F. C., Carbon D. F., Augason G., Wooden D., Bregman J., Goorvitch D., 1992a, AJ, 104, 2045
- Dudley C. C., Wynn-Williams C. G., 1993, ApJ, 407, L65
- Dudley C. C., Wynn-Williams C. G., 1997, ApJ, 488, 720
- Duley W. W., 1989, in Allamandola L. J., Tielens A. G. G. M., eds, Proc. IAU Symp. 135, Interstellar Dust, Kluwer, Dordrecht, p. 141
- Ellis K., Guillois O., Nenner I., Papoular R., Reynard C., 1994, in Nenner I., ed, Molecules and Grains in Space, New York, Amer. Inst. Phys., p. 811
- Genzel R., Becklin E. E., Wynn-Williams C. G., Moran J. M., Reid M. J., Jaffe D. T., Downes D., 1982, ApJ, 255, 527
- Hanner M. S., Brooke T. Y., Tokunaga A. T., 1995, ApJ, 438, 250
- Kalas P., Wynn-Williams C. G., 1994, ApJ, 434, 546
- Keto E., Ball R., Arens J., Jernigan G., Meixner M., Skinner C., Graham J., 1993, ApJ, 413, L23
- Kurucz R. L., 1979, ApJS, 40, 1
- Mathis J. S., 1990, ARA&A, 28, 37
- Piña R. K., Jones B., Puetter R. C., Stein W. A., 1992, ApJ, 401, L75
- Puget L. J., Léger A., 1989, ARA&A, 27, 161
- Puxley P. J., Brand P. W. J. L., 1995 MNRAS 274 L77
- Roche P. F., 1989, in Kaldeich B. A., ed, Proc. 22 Eslab Symposium on Infrared Spectroscopy in Astronomy, ESA, Paris, p. 79
- Roche P. F., Aitken D. K., 1985, MNRAS, 213, 789
- Roche P. F., Aitken D. K., Smith C. H., 1989, MNRAS, 236, 485
- Roche P. F., Aitken D. K., Smith C. H., 1991a, MNRAS, 252, 282
- Roche P. F., Aitken D. K., Smith C. H., Ward M. J., 1991b, MNRAS, 248, 606
- Rubin R. H., 1985, ApJS, 57, 349
- Sakata A., Wada S., 1989, in Allamandola L. J., Tielens A. G. G. M., eds, Proc. IAU Symp. 135, Interstellar Dust, Kluwer, Dordrecht, p. 191
- Sams B. J., Genzel R., Eckart A., Tacconi-Garman L., Hofmann R., 1994, ApJ, 430, L33
- Telesco C. M., Harper D. A., 1980, ApJ, 235, 392
- Tokunaga A. T., 1984, AJ, 89, 172
- Tully R. B., 1988, Nearby Galaxies Catalog, Cambridge University Press, Cambridge
- Turner J. L., Ho P. T. P., 1985, AJ, 299, L77
- Ulvestad J. S., Antonucci R. R. J., 1997, ApJ, 488, 621
- Vigroux L., et al., 1996, A&A, 315, L93
- Watson A. M., et al., 1996, AJ, 112, 534
- Wynn-Williams C. G., 1982, in Kessler M. F., Phillips J. P., eds, Galactic and Extragalactic Infrared Spectroscopy, Dordrecht, Reidel, p. 133
- Zavagno A., Cox P., Baluteau J. P., 1992, A&A 259 241

**Figure 1.** The positions and apertures for the spectra presented in this paper are shown as open circles and labeled P0, P1, P2a, and P2b. The filled circles are the positions of compact radio sources measured by Turner Ho (1985), with the larger two labeled according to their table 2. Kalas & Wynn-Williams's Peak 3 is also labeled. This map is adapted from the 4.8  $\mu\text{m}$  map of Kalas & Wynn-Williams (1994).

**Figure 2.** The 8–13  $\mu\text{m}$  spectra at four positions in the starburst nucleus of NGC 253 are labeled as in Table 1. Large filled circles represent observed data points, while small filled circles, when present, indicate boxcar smoothed data, where the smoothing radius is 0.1  $\mu\text{m}$ . The solid lines are blackbody fits between 10 and 11  $\mu\text{m}$  and at 13  $\mu\text{m}$ . The temperature of the fitted blackbody is indicated in each panel. The dashed lines show a fit of the Orion Bar spectrum (Roche 1989) between 10.9 and 11.7  $\mu\text{m}$ , while the shaded regions indicate the expected range in the strength of the 7.7  $\mu\text{m}$  feature based on the strength of the 11.3  $\mu\text{m}$  feature.

**Figure 3.** The continuum subtracted 10–13.3  $\mu\text{m}$  spectra corresponding to Fig. 2 are presented. The filled circles are the continuum-subtracted data displayed on linear scales in  $F_\lambda$  and wavelength, with 1  $\sigma$  errors that do not include uncertainties in the continuum subtraction. The solid lines give the total model fits for each spectrum. The dot-dashed line in the P0 spectrum indicates the contribution of the plateau and 12.7  $\mu\text{m}$  feature that are subtracted from the [Ne II] flux.

**Figures for  
8-13  $\mu\text{m}$  spectroscopy of NGC 253:  
a spatially resolved starburst**

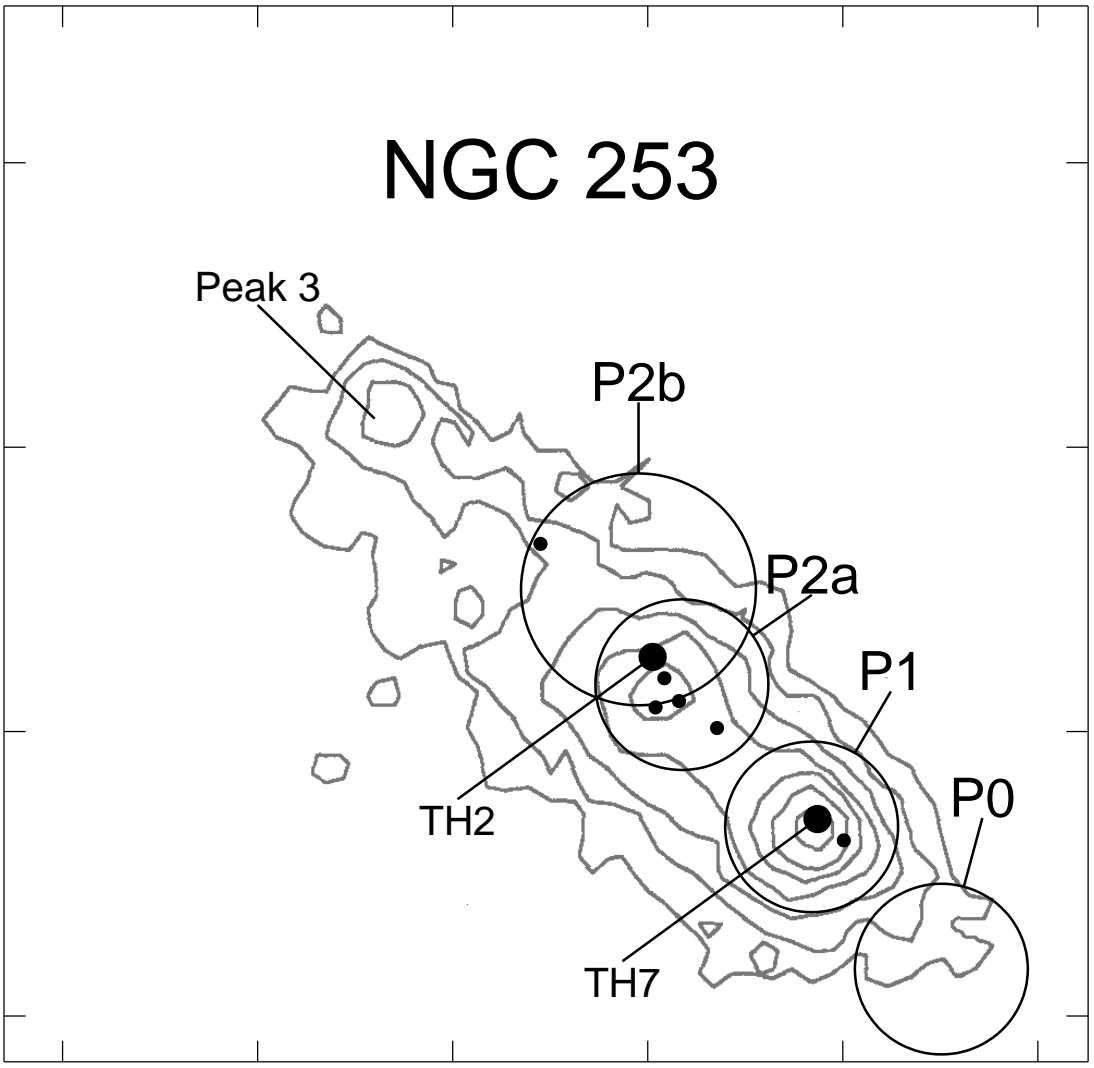
C. C. Dudley & C. G. Wynn-Williams

*Institute for Astronomy, University of Hawaii, 2680 Woodlawn Dr., Honolulu, Hawaii 96822, USA*

# NGC 253

Decination (1950):  $-25^{\circ} 33'$

32"  
36"  
40"  
44"



6<sup>s</sup>.4    6<sup>s</sup>.2    6<sup>s</sup>.0    5<sup>s</sup>.8    5<sup>s</sup>.6    5<sup>s</sup>.4  
Right Ascension (1950): 00<sup>h</sup> 45<sup>m</sup>

